Journal of Materials Science Research and Reviews

Volume 7, Issue 3, Page 380-391, 2024; Article no.JMSRR.120578

Visible Light Induced Photodegradation of Methylene Blue Dye Over ZnO Modified α-Fe_2O_3 Nanocomposites

M.J. Pawar [a*], A.D. Khajone [a] and M.D. Gaonar [a]

[a] Department of Chemistry, Laboratory of Materials Synthesis, Smt. Narsamma Arts, Commerce and Science College, Kiran Nagar, Amaravati, M.S. Bharat 444606, India.

Authors' contributions

This work was carried out in collaboration among all authors. All authors read and approved the final manuscript.

Article Information

Open Peer Review History:
This journal follows the Advanced Open Peer Review policy. Identity of the Reviewers, Editor(s) and additional Reviewers, peer review comments, different versions of the manuscript, comments of the editors, etc are available here: https://www.sdiarticle5.com/review-history/120578

Original Research Article

Received: 01/06/2024
Accepted: 03/08/2024
Published: 07/08/2024

ABSTRACT

The present investigation aimed to synthesize Zinc (Zn) modified hematite (α-Fe_2O_3) nanocomposites with varying concentrations (pure, 10 wt%, 15 wt%, and 20 wt%) via the modified sol-gel method. The influence of dopants on structural and optical properties and photocatalytic activity of hematite was studied. The X-ray diffraction (XRD) pattern of synthesized samples was indexed to rhombohedral hematite with a crystallite size of 15–25 nm. Moreover, these materials were characterized by FTIR spectroscopy and scanning electron microscopy (SEM). The surface morphology of prepared nanoparticles was explored using scanning electron microscopy (SEM). The specific surface area of the solids was calculated by Brunauer–Emmett–Teller (BET) method. Photocatalytic properties of nanoparticles were performed for methylene blue (MB) dye and showed

**Corresponding author: Email: mjpa1809@gmail.com; pawarmahendrasingh22@gmail.com;*

Cite as: *Pawar, M.J., A.D. Khajone, and M.D. Gaonar. 2024. "Visible Light Induced Photodegradation of Methylene Blue Dye Over ZnO Modified α-Fe2O3 Nanocomposites". Journal of Materials Science Research and Reviews 7 (3):380-91. https://journaljmsrr.com/index.php/JMSRR/article/view/339.*

effective degradation in the presence of UV light. Hence, Zn2+ doped hematite can be considered an efficient material for potential applications as a photocatalyst. Zn-doped hematite is developed as a superior photocatalyst for the degradation of MB dye in the presence of UV light.

Keywords: α-Fe_2O_3; Zn-doped α-Fe_2O_3; nanocomposites; photodegradation.

1. INTRODUCTION

"Photocatalytic degradation of organic dyes in wastewater using metal oxide semiconductors has been considered one of the most promising approaches to solving environmental pollution problems [1-5]. Significantly, metal oxide semiconductors (like TiO_2, ZnO, Nb_2O_5, WO_3, Fe_2O_3, etc.) have been investigated as photocatalysts due to their potential characteristics, including high degradation efficiency, environment-friendly, thermal stability, abundance, environment-friendly, recyclable visible-light photocatalysis and low-cost products" [6-12].

"Ferrous oxide (Fe_2O_3) appears in four crystallographic phases, namely hematite (α-Fe_2O_3), maghemite (γ-Fe_2O_3), β-Fe_2O_3, and ε-Fe_2O_3. The thermodynamically stable hematite phase of Fe_2O_3 is a functional semiconductor with a bandgap of 2.1 eV which is environmentally friendly, non-toxic, and important in various fields. Among them, hematite (*α*-Fe_2O_3) has been investigated extensively because it possesses many attractive features, such as ease in handling, chemical stability, nontoxicity, an environment-friendly product, high resistance to corrosion features, and the most stable iron oxide under ambient conditions" [13-15]. "The *α*-Fe_2O_3 can absorb visible light since it has a narrow bandgap ($E_g \approx 2.1$ eV) compared to TiO_2, ZnO, and WO_3 materials. Hematite is a widely investigated material due to its various applications in the fields of photocatalysts, pigments, gas sensors, solar cells, electrochemical sensors, lithium-ion batteries etc. Since the structural and crystallographic forms are generally responsible for their properties, many methods for the synthesis of *α*-Fe_2O_3 including hydrothermal synthesis, forced hydrolysis, combustion method, microwave irradiation method, spray pyrolysis, chemical vapor deposition, pulsed laser deposition, co-precipitation, and high vacuum evaporation and sol-gel is mainly interesting method due to its low cost, high purity, short preparation time, homogeneous solution of doping element and magnify the excellent polycrystalline samples. By doping different metal oxides, it will amplify to find new applications and improve the performance of any other applications. Many researchers have focused on developing mixed oxide semiconductors due to an efficient charge separation obtained by coupling two semiconductor particles with different energy levels" [16-19]. "The improvement in the efficiency of photocatalytic reactions is explained as the result of a vectorial transfer of photo-generated electrons and holes from one semiconductor to another" [20,21]. "Zn-doped hematite materials were synthesized using a modified sol-gel method. ZnO possesses electronic properties and a bandgap energy that is similar to that of TiO_2. It has been reported to be more efficient than TiO_2 in the photooxidation of pollutants" [22,23].

"The photocatalytic activity of metal oxides depends on the preparation method, which affects the physicochemical properties of the solids. The sol-gel method is a convenient approach for tailoring transition metal oxides for specific applications. The sol-gel method offers the advantage of achieving homogeneous mixing of transition metal cations at the molecular level. This enhances the formation of polycrystalline particles with unique properties" [24]. In this study, we synthesized and characterized mixed photocatalyst Zn-doped α-Fe_2O_3 nanocomposites with varying concentrations (pure, 10, 15, and 20 wt%) using a modified sol-gel method. We evaluated the activities of the catalysts by testing their effectiveness in the photocatalytic degradation of MB dye in aqueous solutions.

2. MATERIALS AND METHODS

2.1 Materials

Zinc-doped α-Fe_2O_3 nanoparticles were synthesized using reagents without any purification. The precursors used were $Fe(NO_3)_3 \cdot 9H_2O$ and $Zn(NO_3)_2 \cdot 6H_2O$ in stoichiometric ratios. Diethylamine was used as a reagent, and saturated ammonia solution was used as a precipitating agent. Double-distilled water was used as the reaction medium.

2.2 Synthesis of pure and Zn doped α-Fe_2O_3 Nanoparticles

An aqueous solution containing iron nitrate and zinc nitrate at specified weight ratios (10:90, 15:85, and 20:80) was prepared by dissolving them in 100 ml of double distilled water. The mixture underwent magnetic stirring for 4 hours. Diethylamine was then added to the solution, followed by continued stirring for an additional 2 hours. A saturated solution of ammonium hydroxide was subsequently introduced, and the mixture was stirred at 75°C for another 2 hours, resulting in the formation of a brown-colored solution. After filtration, the solution was thoroughly washed with water and ethanol. The filtered material was dried at 350°C in an oven to yield a gel, which was further subjected to calcination at 450°C and 500°C for 3 hours each.

2.3 Characterization

The synthesized nanocomposites underwent characterization using various spectroscopic techniques such as X-ray diffraction (XRD), Fourier Transform Infrared Spectroscopy (FTIR), scanning electron microscopy (SEM), and UV-visible spectroscopy. The surface area and pore size were determined by analyzing the N_2 adsorption-desorption isotherm and BJH method using a Micromeritics Analyzer (ASAP 2460) at 77 K.

A series of experiments were conducted to evaluate the photocatalytic degradation of MB dye using a photoreactor under UV light irradiation. The light source utilized for photocatalysis was visible light (40 W Hg lamp). After the photocatalytic process, the catalysts and solution were separated via filtration, and the collected samples were analyzed using a UV-Vis spectrophotometer (Shimadzu UV-2450).

The efficiency of photodegradation for RB5 was determined using the following formula:

$$\% \text{ Degradation efficiency} = \frac{C_o - C_t}{C_o} \times 100$$

Where, C_o is the original MB dye concentration, C_t is the retained MB dye concentration.

3. RESULTS AND DISCUSSION

3.1 X-ray Diffraction

The structural analysis and phase identification of synthesized materials were verified using X-ray diffraction (XRD) technique and presented in Fig. 1. Only hematite diffraction peaks were observed, indicating that zinc atoms were successfully incorporated into the Fe_2O_3 matrix. This incorporation did not disrupt the rhombohedral structure of hematite, demonstrating that the dopant atoms altered the crystallinity.

The crystal structure of the zinc-doped hematite nanocomposites was determined and confirmed using an X-ray diffraction meter (Model Miniflex 600, RIGAKU, Japan) with Cu Kα radiation (λ = 1.5405 Å) across a wide range of Bragg angles. The crystalline size was calculated based on the peak widths of the XRD patterns, ensuring minimal non-uniform strains. The particle size of the synthesized samples was estimated using Scherrer's equation [24], which is formulated as:

$$D = \frac{0.95\lambda}{\beta cos\theta}$$

where λ is the X-ray wavelength, β is the full width at half maximum (FWHM) and θ is the diffraction angle, D is the average crystalline size perpendicular to the reflecting angle [25].

The peaks at 2θ values of 24.27, 33.34, 35.80, 41.00, 49.64, 54.18, 62.66, and 64.17 correspond to the lattice planes (012), (104), (110), (113), (024), (116), (214), and (300) respectively. These peaks indicate that the synthesized nanoparticles are in the hematite phase with a rhombohedral structure, as confirmed by JCPDS card No. 89-8104. The average crystallite size of the nanoparticles was estimated using the Debye-Scherrer equation and found to be 35 ± 20 nm. Additionally, a secondary phase corresponding to the (110) plane confirms the incorporation of Zn into the Fe_2O_3 lattice. When the zinc content was increased to 15%, the crystallinity of synthesized materials decreased, suggesting that more strain was introduced into the Fe2O3 lattice.

3.2 Scanning Electron Microscopy (SEM)

Fig. 2 shows the SEM micrographs of Zn-doped samples, revealing cluster formations with crystalline characteristics. The images depict spherical structures ranging in size from 15 to 35 nm with irregular surface morphologies. The stony appearance is likely due to the aggregation of nanoparticles.

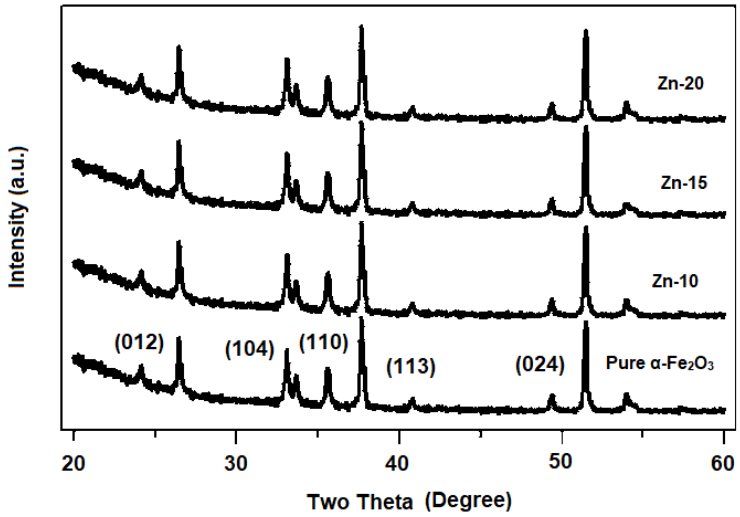

Fig. 1. XRD pattern of pure and Zn doped α-Fe_2O_3materials

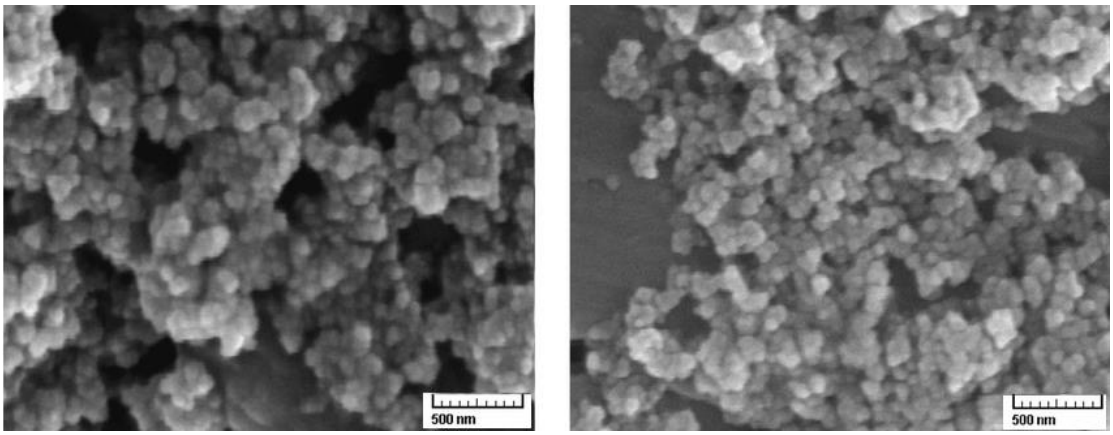

Fig. 2. SEM images of Zn-doped samples

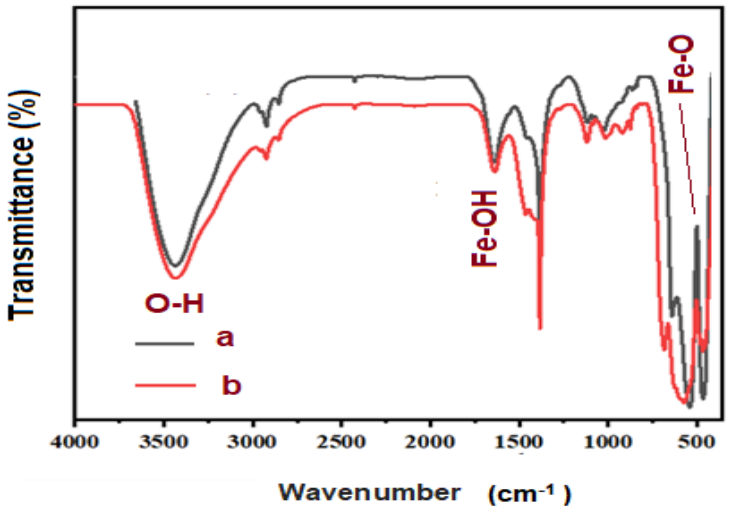

Fig. 3. FT-IR spectra of (a) pure α-Fe_2O_3 and (b) Zn-15 sample

3.3 FT-IR Studies

The presence of functional groups absorbed on the surface of synthesized pure and Zn-doped hematite nanocomposites was determined using FT-IR spectroscopy. The FT-IR spectra of pure Zn-doped hematite calcined at 550°C are shown in Fig. 3. As depicted in Fig. 3, distinctive bands are observed at 3446, 1642, 571, and 478 cm^{-1}. The characteristic Fe-O peaks appear sharply at 478 and 571 cm^{-1}, while the broadband at 3446 cm^{-1} corresponds to the O-H stretch of water molecules. In the regions around 3430 cm^{-1} and 1639 cm^{-1}, observed absorption bands are attributed to the stretching and bending vibrations of water molecules. The bands at 571 cm^{-1} and 478 cm^{-1} are caused by the presence of the dopant and the Fe-O vibrational mode of hematite nanoparticles, confirming the hematite phase in the rhombohedral lattice.

3.4 UV-Vis Absorption Spectrum

The size of particles significantly affects the properties of nanomaterials. Therefore, monitoring the size evolution of semiconducting nanoparticles is crucial for understanding their properties. UV-visible absorption spectroscopy is a commonly used technique for analyzing the optical properties of nanosized particles. Fig. 4 presents the absorption spectra of pure α-Fe_2O_3 and Zn-doped α-Fe_2O_3 nanocomposites. As shown in Fig. 4, the absorption spectra of synthesized hematite in the UV-Vis range exhibit strong absorption between 500 and 700 nm. This observation is consistent with data reported in other studies [5-7]. The optical bandgap (Eg) of nanoparticles can be assessed by extrapolating from the absorption edge, according to the following equation:

$$(\boldsymbol{ahv})^{\boldsymbol{n}} = \boldsymbol{A}\,(\boldsymbol{hv} - \boldsymbol{E_g})$$

Where α is the absorption coefficient, *A* is constant, *h* is the energy of light and *n* is a constant depending on the nature of the electron transition.

3.5 BET Analysis

The surface areas and porosities of the as-synthesized nanomaterials were quantitatively assessed using nitrogen adsorption BET). Before measuring the N_2 adsorption–desorption isotherms at −196°C, the samples were degassed at 150°C for 45 hours. The Brunauer-Emmett-Teller (BET) surface areas, pore volumes, and pore sizes of the synthesized samples are detailed in Table 1. Notably, the Zn-doped α-Fe_2O_3 materials exhibited increased surface area, pore volume, and pore size compared to pure α-Fe_2O_3. It is important to highlight that photocatalytic performance is influenced by surface area, pore size, and pore volume; a greater pore volume, porosity, and surface area enhance the catalyst's ability to interact with and adsorb pollutants.

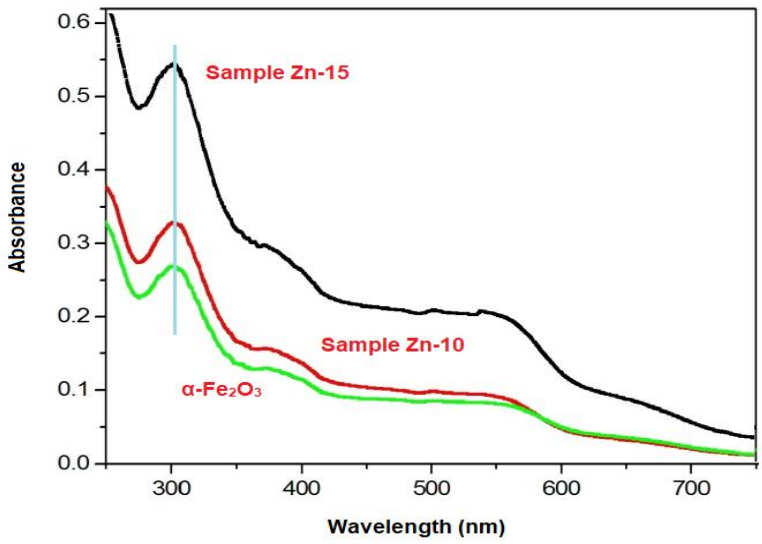

Fig. 4. UV-Vis spectra of synthesized pure and Zn-doped Fe_2O_3 samples

Table 1. Summary of BET-specific surface area, pore volume, and pore size of the as-synthesized samples

Sample	BET specific surface area ($m^2\ g^{-1}$)	Pore volume (cm^3/g)	Pore size (A)
Pure α-Fe_2O_3	12.523	0.0121	29.2
Zn-10	16.569	0.0132	31.5
Zn-15	34.543	0.0456	42.2
Zn-20	17.459	0.0143	30.4

3.6 Photocatalytic Studies

Hematite is a semiconductor with a bandgap of 2.0–2.6 eV and can absorb light from the visible to UV regions of the solar spectrum at specific wavelengths [26]. Therefore, the synthesized nanomaterials could serve as efficient photocatalysts for the rapid degradation of dyes. In this study, we evaluated the photocatalytic activity of the prepared nanoparticles under UV light irradiation using a Methylene Blue (MB) aqueous solution as a model contaminant. Methylene Blue dye is odorless, solid at room temperature, and appears as a dark green powder that turns blue when dissolved in water. MB, a Phenothiazine dye, is extensively used in dyeing and printing industries and has severe toxic effects on human health. UV-visible spectroscopy reveals that MB has three absorption maxima at 246 nm, 291 nm, and 663 nm. The absorption maxima at 291 nm and 663 nm are commonly used for the photodegradation of MB dye. The concentration of the MB dye, in terms of absorbance, was measured at 663 nm (λmax for Methylene Blue) before and after photocatalytic degradation. To elucidate the effect of ZnO wt% on the photocatalytic activity of the α-Fe_2O_3 photocatalyst, parallel experiments were conducted with synthesized photocatalysts containing different ZnO wt%. We investigated various operating parameters, such as Zn doping, pH, catalyst loading, initial dye concentration, oxygen bubbling, and direct solar light, on the photodegradation of MB dye.

The progress of the photocatalytic reaction was monitored by measuring absorbance at regular time intervals. It was found that hematite nanoparticles synthesized with higher dopant concentrations exhibited higher removal efficiencies. The absorbance of MB dye decreased in the presence of the as-synthesized materials and UV light, as shown in Fig. 5. The plot of absorbance versus time was linear, indicating that the reaction followed pseudo-first-order kinetics. The pseudo-first-order kinetic equation is presented below:

$$\ln \frac{C_O}{C_t} = kt$$

Where C_o and C_t are the concentrations of dye in solution at times 0 and t respectively, and k is the first-order rate constant (min^{-1}). It can be predicted from Fig. 5, that after 100 minutes maximum degradation of MB dye was achieved for pure α-Fe_2O_3 sample.

3.6.1 Effect of Zn-doping

The photocatalytic efficiency of Zn-doped α-Fe_2O_3 photocatalysts depends on their ability to generate ·OH radicals in an aqueous solution under irradiation. The concentration of dopants in host metal oxide influences the production of ·OH radicals. Fig. 5 shows that as the Zn concentration increases, the degradation efficiency of MB dye improves over time, with the highest efficiency achieved with Zn-15 in 72 minutes. This indicates that Zn-doped α-Fe_2O_3 nanoparticles could be effective photocatalysts for removing methylene blue pollutants from industrial effluents.

3.6.2 Effect of Catalyst dose

The effect of varying catalyst doses on the photodegradation of MB dye was investigated, with the results shown in Fig. 5. In this study, the dose of pure and Zn-doped α-Fe_2O_3 nanocomposites was varied from 100 to 400 mg/L for an initial dye concentration of 20 mg/L at pH 2, using UV light as the irradiation source. The findings presented in Fig. 5 reveal that the degradation percentage increased with catalyst dosage up to a certain point. However, increasing the catalyst dosage beyond this point resulted in a decrease in dye degradation. The most effective catalyst dosage was determined to be 200 mg/L.

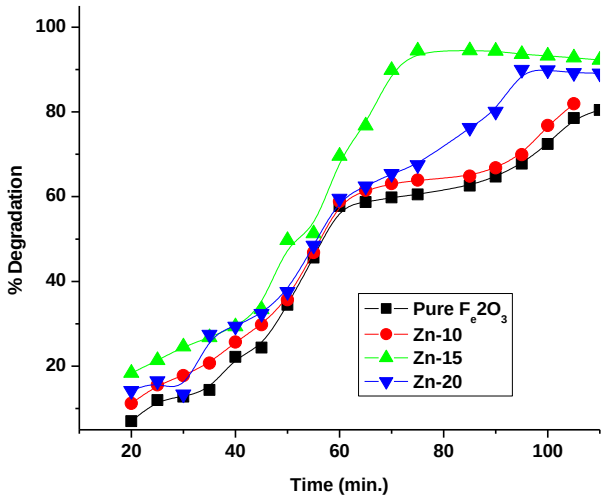

Fig. 5. Photodegradation of MB dye using pure and doped α-hematite

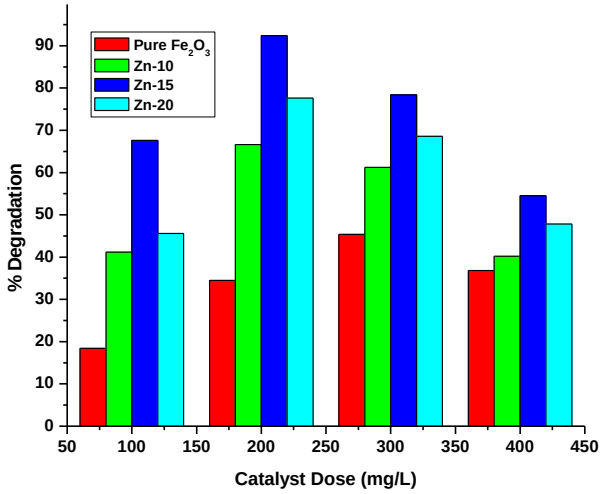

Fig. 6. Effect of catalyst dosage on MB dye degradation

The initial increase in percent degradation is likely due to a rise in the number of active sites on the catalyst's surface with a higher catalyst dosage. As the dosage increases, the concentration of free radicals, such as •OH and O_2^{2-}, in the solution also rises, enhancing the photodegradation of the wastewater sample [22]. However, additional increases in catalyst dosage resulted in reduced photodegradation due to the excessive amount of catalyst. At this stage, the catalyst particles start to clump together, decreasing the amount of sunlight that reaches the active sites and thus reducing the reaction rate. This finding is consistent with prior research [23-24].

3.6.3 Effect of pH

In photocatalytic studies, pH is essential for controlling the reactions related to the degradation of organic compounds and influences the generation of hydroxyl radicals [20,21]. Initially, the impact of pH on the photocatalytic degradation of MB dye was investigated across a pH range of 1–10 using the synthesized nanomaterials, with conditions set at a contact time of 120 minutes, a dye

concentration of 20 mg/L, and a catalyst dose of 1 g/L, as shown in Fig. 7. The pH of the solution influences the surface charge properties of the catalyst, which in turn affects the adsorption behavior of the photocatalyst [22].

The percentage of dye removal increased as the pH value decreased, peaking in the acidic range at pH 2. At lower pH values, the surfaces of the catalysts became highly protonated and positively charged, which enhanced the electrostatic attraction of dye cations to the catalyst surface. This increase in oxidizing holes resulted in improved degradation of MB dye. In acidic conditions positive holes serve as the primary oxidation species, while hydroxyl radicals are the predominant species at neutral or alkaline pH levels [24]. The maximum degradation of MB dye was achieved at pH 2, with pure α-Fe_2O_3 and Zn-15 samples showing degradation rates of 74.6% and 92.8%, respectively.

3.6.4 Effect of initial dye concentration

The impact of initial dye concentration on degradation efficiency was examined at an optimized pH of 2 with a fixed catalyst dose by varying the initial dye concentration. MB dye concentrations ranging from 10 to 50 mg/L were tested to evaluate photocatalytic activity. Fig. 8 illustrates that maximum dye degradation occurred at an initial concentration 20 mg/L. It was observed that as the initial dye concentration increased, the degradation efficiency decreased. This is because a higher dye concentration leads to an excess of dye molecules adsorbed onto the catalyst surface, reducing the availability of active sites. As the dye concentration increases, more hydroxyl radicals are required for degradation. However, the production of hydroxyl radicals on the catalyst surface remains constant for a fixed light intensity, catalyst dose, and irradiation time [27]. As a result, at higher dye concentrations, the number of available hydroxyl radicals becomes inadequate for effective degradation, resulting in decreased photodegradation efficiency.

3.6.5 Effect of bubbling oxygen

To assess the impact of oxygen bubbling on photocatalytic efficiency, MB dye degradation was evaluated by introducing oxygen into an aqueous suspension containing 20 mg/L of dye and 1 g/L of Zn-15 catalyst. Degradation experiments were also performed in a deoxygenated medium by removing oxygen through nitrogen bubbling for 30 minutes, and then sealing the reactor with a septum to prevent external interactions. The results, shown in Fig. 9, demonstrate that degradation performance is significantly higher in the oxygenated environment compared to the non-oxygenated medium. Specifically, the degradation yield of MB dye with oxygen was around 98.5%, while it was approximately 92.4% in the absence of oxygen.

3.6.6 Solar light photodegradation of MB dye

Solar radiation offers the benefit of being an abundant and environmentally friendly energy source. However, the two photocatalysts absorb only a small fraction of the total sunlight. It is valuable to investigate the photocatalytic degradation of an aerated MB solution with the Zn-15 sample, as shown in Fig. 10. For this experiment, we used a similar approach to UV irradiation but exposed the MB dye (20 mg/L) solution directly to solar radiation (sunlight intensity at 355 nm). Photodegradation of MB under direct sunlight began to show progress after 55 minutes of exposure. Due to the substantial amount of light absorbed by the photocatalyst, the degradation process accelerated after 120 minutes.

3.6.7 Reusability of photocatalyst

Currently, recovery and reusability are crucial factors in choosing a cost-effective and practical catalyst for pilot-scale remediation systems.

The reusability of the synthesized nanomaterials was assessed over seven cycles of MB dye photodegradation using 100 mL of a 20 mg/L MB dye solution at pH 2 with a catalyst dose of 1 g/L. Fig. 11 shows the recyclability and stability of the Zn-15 catalyst after seven cycles, each lasting 70 minutes. The Zn-15 catalyst was easily recyclable using a strong magnet and could be reused. After seven cycles, the photoactivity of the Zn-15 catalyst declined by 5%, yet it maintained high efficiency. This minor reduction in photocatalytic activity can be attributed to several factors: (i) Material loss during washing and drying led to a reduced dose in subsequent cycles, diminishing surface catalytic activity and overall performance [24]. (ii) Nanoparticle aggregation decreased the effective surface area and the number of active sites, potentially causing fouling and performance changes over multiple cycles [28]. (iii) The catalyst's surface activity progressively decreased due to the accumulation of catechol and its intermediates, which blocked the pores and active sites after each cycle [29].

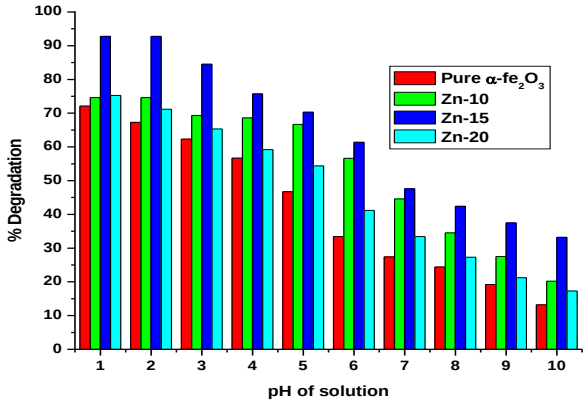

Fig. 7. Effect of pH on photodegradation of MB dye

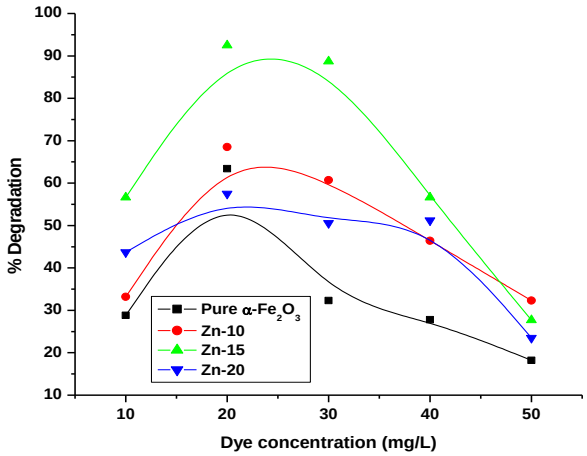

Fig. 8. Effect of dye concentration on dye degradation at pH 2

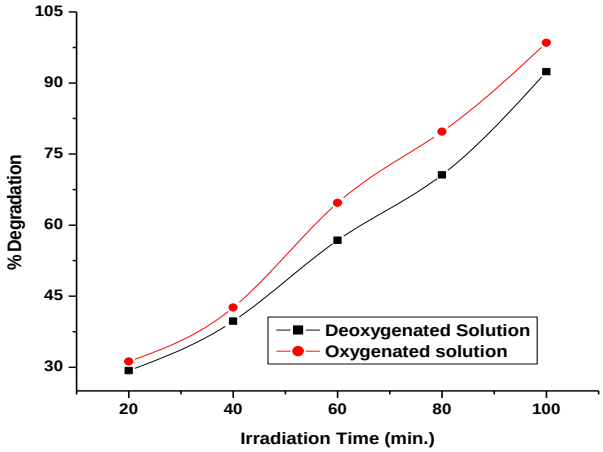

Fig. 9. Degradation of MB as a function of irradiation time in oxygenated and deoxygenated aqueous medium

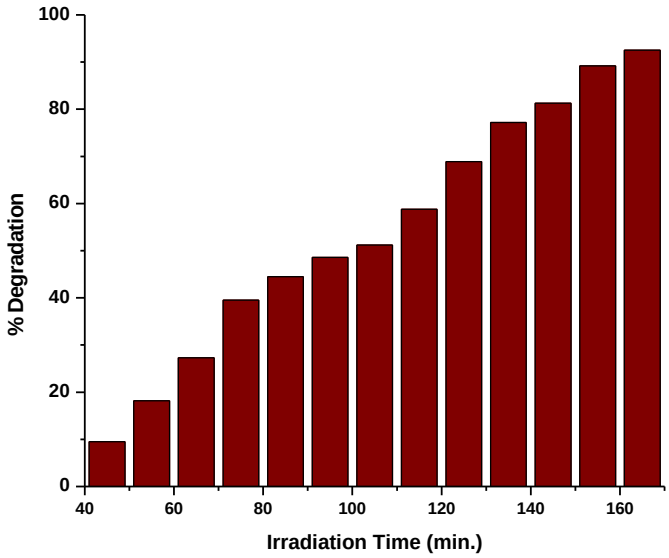

Fig. 10. Kinetics of the MB dye (20 mg/L) photocatalytic degradation using sample Zn-15 with solar light irradiation

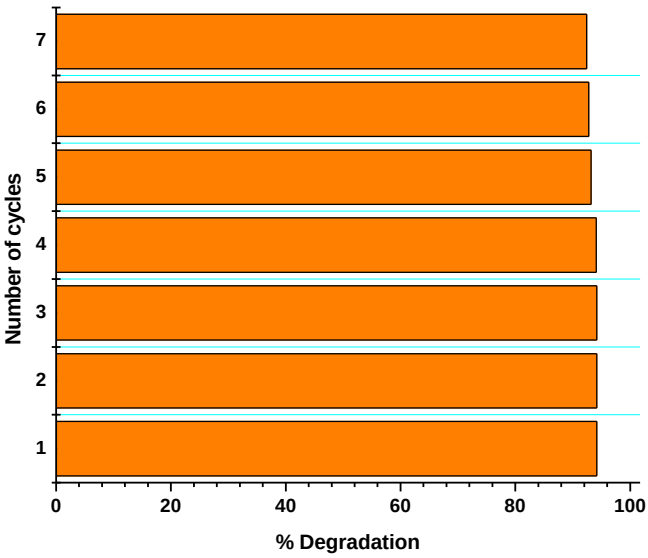

Fig. 11. Reusability function of Zn-15 sample for degradation of MB dye

4. CONCLUSION

In this report, Zn-doped α-Fe_2O_3 nanocomposite is synthesized through a thermal decomposition method and then applied for the photocatalytic degradation of methylene blue (MB) dye. The as-synthesized catalyst was characterized by XRD, revealing that the doped Zn was effectively integrated into the structure. However, a shift in 2θ values towards higher angles was observed. SEM results showed the sphere-shaped morphology of the catalyst in the range of 27-52 nm in size. The surface area of as-synthesized Zn doped α-Fe_2O_3 nanocomposite was found to be 16.569, 34.543, and 17.459 m^2/g, and that for pure is 12.523 m^2/g through the BET analysis.

The Zn-doped α-Fe_2O_3 nanocomposite was found to have an improved degradation efficiency than the catalyst when used under visible light, and it showed about 92.81% degradation of MB dye within 150 minutes. The degradation of MB dye was investigated by varying parameters such as catalyst dose, pH, initial dye concentration, and the introduction of O_2 through bubbling. Then the reusability of the catalyst was studied by performing a cyclic test, and the catalyst showed good photocatalytic activity up to seven consecutive cycles. From the results obtained, we propose a Zn-doped α-Fe_2O_3 nanocomposite as an efficient photocatalyst for the degradation of organic dyes, and it can be applied to other organic pollutants in the future.

DISCLAIMER (ARTIFICIAL INTELLIGENCE)

Author(s) hereby declare that NO generative AI technologies such as Large Language Models (ChatGPT, COPILOT, etc) and text-to-image generators have been used during writing or editing of manuscripts.

COMPETING INTERESTS

Authors have declared that no competing interests exist.

REFERENCES

1. Zhang YJ et al. Alkali-activated cements for photocatalytic degradation of organic dyes. In: Handbook of Alkali-Activated Cements, Mortars and Concretes. Elsevier: Amsterdam. 2015;729.
2. Zhang YJ et al. A facile and low-cost synthesis of granulated blast furnace slag-based cementitious material coupled with Fe_2O_3 catalyst for treatment of dye wastewater. Appl. Catal. B, Vols. 2013; 138–139:9–16.
3. Dutta AK, Maji SK, Adhikary B. γ-Fe_2O_3 nanoparticles: An easily recoverable effective photo-catalyst for the degradation of rose bengal and methylene blue dyes in the waste-water treatment plant. Materials Research Bulletin. 2014;49:28–34.
4. Li X, Liu Y, Zhang C, Wen T, Zhuang L, Wang X, Song G, Chen D, Ai Y, Hayat T, Wang X. Porous Fe_2O_3 microcubes derived from metal organic frameworks for efficient elimination of organic pollutants and heavy metal ions. Chemical Engineering Journal. 2018;336:241–252.
5. Guo SQ, Hu Z, Zhen M, Gu B, Shen B, Dong F. Insights for optimum cation defects in photocatalysis: A case study of hematite nanostructures. Applied Catalysis B. 2020;264:118506.
6. Souza JB. Junior Jr., et al, On the relevance of understanding and controlling the locations of dopants in hematite photoanodes for low-cost water splitting. Applied Physics Letters. 2021;119:200501.
7. Rasheed RT et al. Preparation and characterization of hematite iron oxide (α-Fe_2O_3) by sol–gel method. Chemical Sciences Journal. 2018;9:2.
8. Tsege EL, Atabaev TS, Hossain MA, Lee D, Kim H, Hwang Y. Cu-doped flower-like hematite nanostructures for efficient water splitting applications. Journal of Physics and Chemistry of Solids. 2016;98:283–289.
9. Meng QL, Wang Z, Chai X, Weng Z, Ding R, Dong L. Fabrication of hematite (α-Fe_2O_3) nanoparticles using electrochemical deposition. Applied Surface Science. 2016;368:303–308.
10. Cao ZQ, Qin M, Gu Y, Jia B, Chen P, Qu X. Synthesis and characterization of Sn-doped hematite as visible light photocatalyst. Materials Research Bulletin. 2016;77:41–47.
11. Mahmoodi NM. Photocatalytic degradation of dyes using carbon nanotube and titania nanoparticle. Water, Air, and Soil Pollution. 2013;224:1612.
12. Oveisi M, Mahmoodi NM, Asli MA. Facile and green synthesis of metal–organic framework/inorganic nanofiber using electrospinning for recyclable visible-light photocatalysis. Journal of Cleaner Production. 2019;222:669–684.
13. Alagiri M, Hamid SBA. Sol–gel synthesis of α-Fe_2O_3 nanoparticles and its photocatalytic application. Journal of Sol-Gel Science and Technology. 2015; 74:783–789.
14. Sarkar D, Mandal M, Mandal K. Design and synthesis of high performance multifunctional ultrathin hematite nanoribbons. ACS Applied Materials and Interfaces. 2013;5:11995–12004.
15. Maji SK, Mukherjee N, Mondal A, Adhikary B. Synthesis, characterization and photocatalytic activity of α-Fe_2O_3 nanoparticles. Polyhedron. 2012;33:145–149.
16. Valenzuela MA, Bosch P, Jiménez-Becerrill J, Quiroz O, Páez AI. Preparation,

characterization and photocatalytic activity of ZnO, Fe_2O_3 and $ZnFe_2O_4$. Journal of Photochemistry and Photobiology A. 2002;148:177–182.
17. Sene Jeosadeque J et al. Journal of Physical Chemistry. Part B. 2003;107: 1597.
18. Chiang K, Amal R, Tran T. Photocatalytic degradation of cyanide using titanium dioxide modified with copper oxide. Advances in Environmental Research. 2002;6:471–485.
19. Sadeghi M, Liu W, Zhang T, Stavropoulos P, Levy B. Role of photoinduced charge carrier separation distance in heterogeneous photocatalysis: Oxidative degradation of CH_3OH vapor in contact with Pt/TiO_2 and Cofumed $TiO_2{-}Fe_2O_3$. Journal of Physical Chemistry. 1996;100:19466–19474.
20. Ho W, Yu JC, Lin J, Yu J, Li P. Preparation and photocatalytic behavior of MoS2 and WS2 nanocluster sensitized TiO_2. Langmuir. 2004;20:5865–5869.
21. Serpone N. Photochem photobiol. Annali di Chimica. 1995;85:247.
22. Villasenor J et al. J Chem Technol Biotechnol. 1998;13(72):105.
23. Pal B, Sharon M. Enhanced photocatalytic activity of highly porous ZnO thin films prepared by sol–gel process. Materials Chemistry and Physics. 2002;76:82–87.
24. Ding Z, Lu GQ, Greenfield PF. Role of the crystallite phase of TiO_2 in heterogeneous photocatalysis for phenol oxidation in water. Journal of Physical Chemistry B. 2000;104:4815–4820.
25. Sherman DM. Electronic structures of iron (III) and manganese (IV) (hydr) oxide minerals: Thermodynamics of photochemical reductive dissolution in aquatic environments. Geochimica et Cosmochimica Acta. 2005;69:3249–3255.
26. Marathe YV, Ramanna MMV, Shrivastava VS. Synthesis and characterization of nanocrystalline CdS thin films grown by chemical bath deposition at different molarities for removal of methylene blue. Desalination and Water Treatment. 2013;51:5813–5820.
27. Lalithambika KC, et al. Journal of Materials Science: Materials in Electronics. 2017; 282062.
28. Xu J, Sheng GP, Luo HW, Li WW, Wang LF, Yu HQ. Fouling of proton exchange membrane (PEM) deteriorates the performance of microbial fuel cell. Water Research. 2012 Apr 15;46(6):1817-24.
29. Ródenas M, El Haskouri J, Ros-Lis JV, Marcos MD, Amorós P, Úbeda MÁ, Pérez-Pla F. Highly active hydrogenation catalysts based on Pd nanoparticles dispersed along hierarchical porous silica covered with polydopamine as interfacial glue. Catalysts. 2020 Apr 22;10(4):449.

Disclaimer/Publisher's Note: The statements, opinions and data contained in all publications are solely those of the individual author(s) and contributor(s) and not of the publisher and/or the editor(s). This publisher and/or the editor(s) disclaim responsibility for any injury to people or property resulting from any ideas, methods, instructions or products referred to in the content.

© Copyright (2024): Author(s). The licensee is the journal publisher. This is an Open Access article distributed under the terms of the Creative Commons Attribution License (http://creativecommons.org/licenses/by/4.0), which permits unrestricted use, distribution, and reproduction in any medium, provided the original work is properly cited.

Peer-review history:
The peer review history for this paper can be accessed here:
https://www.sdiarticle5.com/review-history/120578